Nanohole Plasmons in Optically Thin Gold Films

Tomas Rindzevicius, Yury Alaverdyan, Borja Sepulveda, Tavakol Pakizeh, and Mikael Käll*

Department of Applied Physics, Chalmers University of Technology, SE-412 96 Göteborg, Sweden

Rainer Hillenbrand

Nano-Photonics Group, Max-Planck-Institut für Biochemie, 82152 Martinsried, Germany

Javier Aizpurua† and F. Javier García de Abajo†,‡

Donostia International Physics Center, Paseo Manuel de Lardizabal 4, Donostia-San Sebastian 20018, Spain, and Instituto de Optica, CSIC, Serrano 121, 28006 Madrid, Spain

Received: September 12, 2006; In Final Form: October 25, 2006

The optical properties of single nanoholes in optically thin ($t = 20$ nm) gold films on glass have been studied experimentally and theoretically. The measured elastic scattering spectra from the nanoholes exhibit a broad resonance in the red part of the visible spectrum, which is qualitatively similar to localized surface plasmon (LSP) resonances in gold nanodisks. The hole resonance red-shifts with increasing hole diameter ($D = 60-107$ nm), similar to particle LSP resonances. These features could be well reproduced by electrodynamic simulations based on the boundary element method (BEM). Further, the electric field distribution around the resonant nanoholes, obtained from the BEM simulations, exhibits a clear electric dipole pattern. This confirms the assignment of the hole resonance to a dipolar LSP resonance mode. However, in comparison with Au nanodisks of similar size, the hole LSP resonance exhibits a shorter dephasing time (τ). This observation can be understood in terms of an additional decay channel that is dominated by the short wavelength antisymmetric bound (a_b) surface plasmon polariton (SPP) mode of the surrounding Au film. Experimental verification of the LSP-SPP coupling is obtained from near-field scanning optical microscopy images, which exhibit interference fringes due to SPP emission from the hole. The fringe periodicity corresponds to a SPP wavelength of $\lambda_{ab} \approx 285$ nm, much less than both the free space wavelength $\lambda_0 = 633$ nm or the wavelength of the more well-known symmetric leaky mode.

1. Introduction

The discovery of enhanced optical transmission through subwavelength hole arrays[1] has attracted considerable interest to optical phenomena and applications associated with nanoscale apertures in metal films.[2−9] It is generally agreed that surface plasmon (SP) resonances play a key role in enhancing the transmission of light through apertures in noble metal films, although diffraction effects, especially in the presence of long-range order, also need to be considered.[10,11] Isolated nanoholes in optically thick metal films exhibit distinct optical properties[12] in comparison to nanohole arrays.[13] In order to make a clear distinction between diffraction and plasmonic coupling effects, a deeper understanding of single nanohole optical properties is needed. Zakharian et al.[14] recently presented a qualitative picture of the behavior of the electromagnetic fields around single elliptical apertures in optically thick metal films. It was argued that electric and magnetic dipoles are induced and that these contribute significantly to the enhanced transmission. Such dipolar modes can be expected to result in localized surface plasmon (LSP) resonances, similar to those observed for noble metal nanoparticles.[15] However, the presence of the metal film obviously constitutes a major difference between a hole and a particle, because a nanohole LSP resonance can be expected to couple not only to ordinary light waves but also to spatially extended surface plasmon polaritons (SPPs). Chang et al.[16] and Popov et al.[17] recently performed electrodynamic simulations which indicated that illumination of a nanohole in an optically thick gold film leads to polarization dependent SPP patterns, in good agreement with experiments using near-field scanning optical microscopy (NSOM).[18]

Concerning holes in optically thin metal films, the key role of surface plasmons has also been invoked.[19] We have previously demonstrated experimentally that isolated and short-range ordered arrays of circular nanoholes in 20 nm thick gold films on glass support excitations that are qualitatively very similar to particle LSP resonances.[20] Similar to particle plasmons, the nanohole resonance was shown to vary with hole diameter D, hole density, and surrounding refractive index. Further, it was argued that these holes allow SPP excitation, which in turn renormalizes the nanohole resonance. However, we were not able to present rigorous experimental proof for LSP-SPP coupling, and the assignment of the hole resonance to an electric dipole LSP mode remained speculative due to the considerable difficulty of performing high quality electrodynamic simulations for this type of nanooptical system. Despite these uncertainties, we were able to use the nanohole structures for advanced sensing applications.[21,22] Short-range ordered nanoholes were utilized in biosensing experiments, in which it was possible to func-

* To whom correspondence should be addressed. E-mail: kall@fy.chalmers.se.

† Donostia International Physics Center.

‡ Instituto de Optica, CSIC.

10.1021/jp065942q CCC: $37.00
Published on Web 12/19/2006

tionalize the inner SiO_2 part of the holes with lipid bilayers for "biomimetic" surface plasmon resonance detection of molecular binding events.[21] This kind of measurement was even possible to perform using a single 60 nm diameter nanohole.[22]

Utilizing alkanethiol self-assembled monolayers, we estimated that the spatial extension of the sensing region was 10−20 nm (i.e., similar to what is expected for nanoparticle LSPs).[22] Still, the development of the nanohole structure into a competitive system for plasmonic bio/chemo sensing requires a more thorough understanding of hole plasmons in thin gold films.

In this paper, we focus on the fundamental optical properties of single nanoholes in optically thin gold films. We compare experimental elastic scattering spectra with simulated spectra obtained using the boundary element method and find excellent agreement. This allows us to analyze the nature of the nanohole excitation through electromagnetic field distribution maps. Moreover, new NSOM data gives indisputable evidence for coupling to extremely short wavelength SPPs, which we identify as so-called antisymmetric bound modes of the thin Au film. The paper is organized as follows. Section II briefly describes the experimental methods used to prepare and study the single nanoholes. In section III, the theoretical models that were employed to simulate the optical properties of the nanoholes are described, whereas section IV discusses results and analyzes the LSP-SPP interaction in single nanoholes. The work is summarized in Section V.

2. Experimental Methods

The single nanoholes were prepared using colloidal lithography[23] on glass substrates. First, colloidal white-sulfate polystyrene spheres (sulfate latex IDC USA) were electrostatically adsorbed on clean glass coverslips. A gold film (20 nm in thickness) is then thermally evaporated onto the colloidal sphere mask, after which the gold-capped spheres are removed by sonication in ethanol. The result is a 20 nm thick gold film containing circular holes with SiO_2 at the bottom. Isolated single nanoholes ($d_{\text{interhole}} \gtrsim 8\ \mu$m) were prepared by kinetically interrupting particle adsorption at extremely low coverage. The diameters of the nanoholes are controlled by choosing the size of the spheres: for this study, we prepared three different samples with average hole diameters 60, 76, and 107 nm, as determined by scanning electron microscopy (SEM) imaging. The variation in hole diameters caused by sphere polydispersity was approximately ±10 nm. The optical properties of the isolated holes were quantified using elastic (Rayleigh) scattering, measured in a dark-field (DF) microscopy setup. A standard inverted optical microscope (Nikon TE300) and an optical spectrometer (AvaSpec-2048) were used. As schematically depicted in Figure 1a, unpolarized white light from a 100 W halogen lamp, A, is focused on the sample, B, using a dark-field condenser (NA = 0.8−0.95, $\theta \approx 53-72$ deg). The scattered light is then collected with a 100× oil immersion objective (NA = 0.5), C, and guided through a fiber to the spectrometer, D. For the objective/fiber combination used, the probe area has a diameter of ∼1.3 μm. Scattering spectra were obtained by first subtracting the background signal obtained from a hole-free region of the Au− film from the raw DF spectra, and then dividing by the white-light spectrum measured under bright-field conditions. Identical conditions were used for different hole samples, so that relative scattering intensities could be determined. Figure 1, panels b and c, shows typical SEM and DF images of single holes.

To complete the experimental methodology, near-field optical imaging of a single 60 nm hole was performed by a scattering-type near-field scanning optical microscope (s-NSOM)[24] that employs Pt coated Si tips as light scattering probes. The tip is illuminated from the side by a TM polarized HeNe laser beam (λ = 633 nm). The illumination angle of the slightly focused laser beam is about 40°, measured from the gold surface, and the laser beam illuminates the hole from the air side. The light backscattered from the tip is detected with a heterodyne interferometer yielding amplitude and phase.

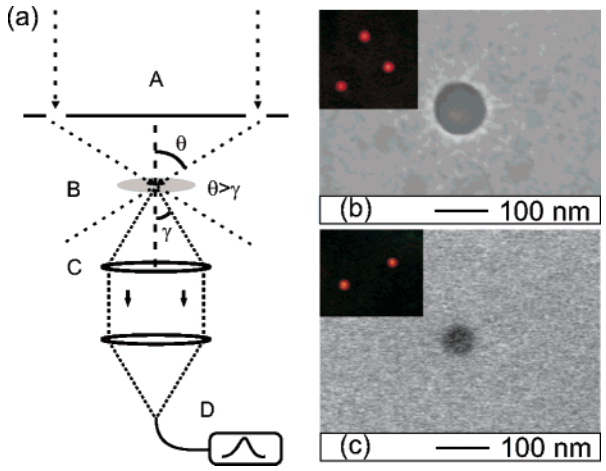

Figure 1. (a) Schematics of the dark-field (DF) setup, (b and c) representative SEM images of single ∼107 and ∼60 nm nanoholes in 20 nm thick gold film, respectively. The insets show corresponding single hole images under DF illumination.

3. Theoretical Methods

Near-field calculations for nanoholes were performed using BEM.[25,26] The electric and magnetic fields are written in terms of scalar and vector potentials ϕ and **A**, and the solution to Maxwell's equations that vanishes away from the hole is expressed in terms of a distribution of charges σ_j and currents $\mathbf{h}_j$ that are defined on either side of all boundaries between the different media. In our case, j = 1, 2, and 3 will label vacuum, gold, and glass, respectively. For **r** inside medium j, one has

$$\phi(\mathbf{r}) = \phi^e(\mathbf{r}) + \int_{S_j} \mathrm{d}\mathbf{s}\, G_j(|\mathbf{r}-\mathbf{s}|)\sigma_j(\mathbf{s}) \tag{1}$$

and

$$\mathbf{A}(\mathbf{r}) = \mathbf{A}^e(\mathbf{r}) + \int_{S_j} \mathrm{d}\mathbf{s}\, G_j(|\mathbf{r}-\mathbf{s}|)\mathbf{h}_j(\mathbf{s}) \tag{2}$$

where S_j refers to the boundary of medium j

$$G_j(|\mathbf{r}-\mathbf{s}|) = \frac{e^{ik_j|\mathbf{r}-\mathbf{s}|}}{|\mathbf{r}-\mathbf{s}|} \tag{3}$$

is the scalar-wave Green function propagator in medium j; $k_j = (\omega/c)\sqrt{\epsilon_j}$ is the momentum of light inside medium j of permittivity ϵ_j; and ϕ^e and $\mathbf{A}^e$ are scalar and vector potentials associated with the incoming light, which are nonvanishing only for j = 1 (i.e., in the medium above the film, which is illuminated by an incoming plane wave). The boundary conditions of the electromagnetic field are then imposed and yield a set of self-consistent surface integral equations that determine the surface sources and that are solved by linear algebra techniques upon discretization of the integrals.[26] The BEM relies on parametrization of finite structures. The near field is thus calculated for films of finite increasing size until convergence is achieved.

The far-field optical response is, however, extremely sensitive to the termination of the film. We have therefore extended the BEM to cope with infinite planar interfaces. In our scheme, the BEM is used to parametrize a hole-like void inside the metal and to calculate forward and backward scattering coefficients for planar and evanescent waves incident from above and from below the hole. These coefficients are regarded as elements of a scattering matrix. The film boundaries lead to diagonal scattering matrices for incident plane waves, whose elements are given by Fresnel's reflection and transmission coefficients. All of these elements (the hole and the film boundaries) are combined into a multiple-scattering scheme, producing the full scattering matrix of the film with the hole-like inclusion. The film boundaries are made increasingly close to the hole until the actual hole-in-a-film structure is realized. Convergence with increasing number of parametrization points in the underlying BEM calculation, with increasing number of planar and evanescent waves, and with decreasing distance between the film boundaries and the hole has been checked. We are interested in the matrix elements that connect the incoming light with transmitted waves. The latter are integrated over all transmission directions, so that the resulting transmission intensity can be compared with dark-field scattering measurements.

In addition to the BEM simulations, we calculated the SPP characteristics for a homogeneous planar 20 nm gold film between glass and air. The calculation of the in-plane wavevector and field distribution of the antisymmetric surface plasmon polariton has been carried out using a transfer matrix formalism.[27] Such a formalism allows us to relate the tangential components of the electromagnetic fields at the two sides of the metallic layer. Since SPPs are transversal magnetic (TM) waves, only the TM field components are required.[27] To calculate the dispersion of the bound antisymmetric mode, we assume that there are no incident plane waves from the surrounding dielectrics. With this condition, a homogeneous system of equations for the amplitudes of the TM field components at both sides of the metal is obtained. The nontrivial solution of the system generates an equation, which solution provides the in-plane wavevector (k) of the bound mode. Once k is calculated, the electromagnetic field distribution in each medium can be determined.

In order to find the complex propagation constants of leaky modes in this lossy waveguide, the reflection pole method was implemented.[28] The technique is based on the transfer matrix method, and it monitors the phase of the reflection coefficient denominator. A numerical differentiation of the phase of the reflection coefficient denominator vs the effective index produces Lorentzian-type peaks (real part of the normalized mode propagation constant). The half width at half-maximum of these peaks is equal to the normalized imaginary part of the mode propagation constants.

4. Results and Discussion

4.1. Optical Properties of Isolated Nanoholes. Using the dark-field spectroscopy setup, it is relatively straightforward to identify individual nanoholes and measure elastic scattering spectra, see insets in Figure 1, panels b and c. Figure 2a shows scattering spectra averaged over 30−40 single nanoholes for each of the three diameters. The spectra are inhomogeneously broadened because of the spread in polystyrene sphere sizes, but the effect is not significant due to the intrinsically large line-width of the individual hole spectra. Consequently, the averaged spectra are well described by Lorentzian line-shapes

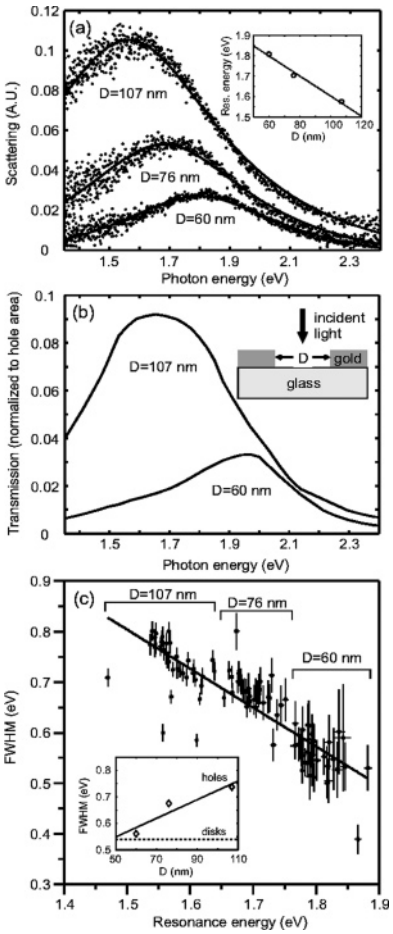

Figure 2. (a) Averaged elastic scattering spectra of 30−40 isolated nanoholes per sample with average diameter of 60, 76, and 107 nm. The spectra are fitted to Lorentzian functions. The inset shows the variation in average resonance energy versus average hole size. (b) Calculated intensity transmitted to the half-space below the hole (see inset) normalized to hole area for 60 and 107 nm holes. (c) Correlation between resonance energy and the full width at half-maximum (fwhm) for the whole ensemble of isolated holes. Inset shows peak width vs hole diameter together with the trend reported for Au nanodisks of similar sizes according to ref 29.

without any Gaussian (inhomogeneous) contribution. The averaged peak positions extracted from the Lorentzian curve fits are 1.80, 1.70, and 1.57 eV for 60, 76, and 107 nm holes, respectively. The hole resonance thus red-shifts monotonously with increased hole diameter, see inset of Figure 2a, in agreement with our earlier investigations[20] and qualitatively similar to gold nanodisks.[29] However, the nanohole spectrum is red-shifted and broader in comparison with that of a nanodisk of identical size.

In a simplified analysis, the LSP resonance position for a nanodisk is determined by the real part of a dipole polarizability denominator, which primarily depends on the disk aspect ratio.[30] However, to the best of our knowledge, an equivalent electrostatic point dipole model for a hole in a thin film has not been formulated. Consequently, the single hole problem has to be treated by rigorous electrodynamic methods that give the solution to Maxwell's equations. In this work, this is done using the BEM. The gold dielectric function was taken from Johnson and Christy.[31] Figure 2b shows the calculated transmission spectra of 60 and 107 nm nanoholes. To illustrate the large increase in the transmission cross section for larger nanoholes, the spectra in Figure 2b were normalized to the geometrical cross-section. The calculated transmission peak positions are

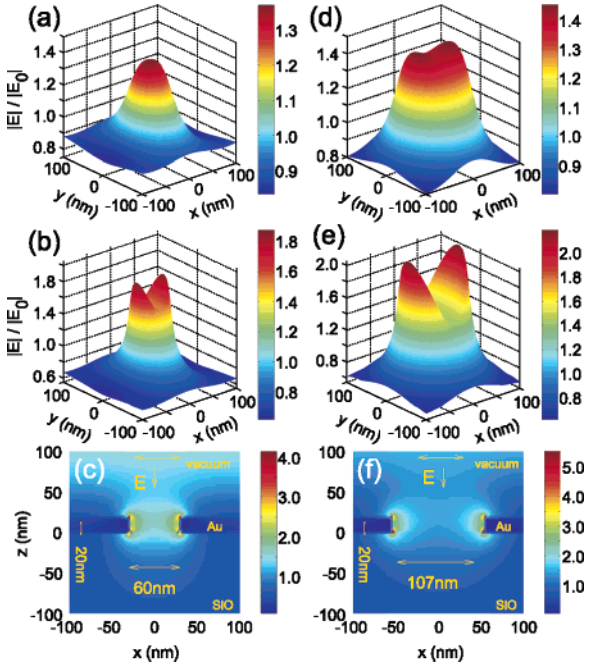

Figure 3. Calculated E-field distribution around 60 nm, (a−c), and 107 nm, (d−f), holes in a 20 nm thick Au film on SiO_2. The near-field plots were made 20 nm (a and d) and 5 nm (b and e) above the hole. The calculations were produced using the BEM, and the normally incident monochromatic light was polarized in the *x* direction.

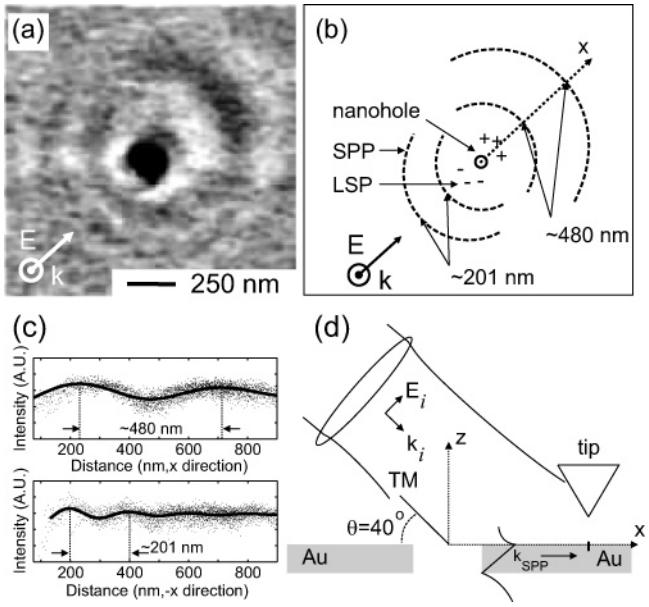

Figure 4. (a) Scattering-type near-field optical image of a single 60 nm nanohole on glass taken with a 40° illumination angle and λ = 633 nm. The beam is TM polarized. (b) Schematic illustration of SPP excitation around a nanohole. (c) Optical signal amplitude as a function of distance from the hole averaged over a cone with 90° opening angle along the *x*-axis. The data was fitted to the expression for the signal amplitude, E_t. (d) Side-view of the s-NSOM experiment.

1.95 eV for D = 60 nm and 1.65 eV for D = 107 nm single holes, in excellent agreement with the experimental spectra. This is a good indication that also the near-field properties of the nanohole resonance can be analyzed using the BEM, as will be discussed below.

As can be seen in Figure 2a, an increase in hole diameter not only leads to a red-shift but also causes spectral broadening; that is, the lifetime of the hole resonance is shortened. This is in contrast to gold nanodisks, for which the LSP lifetime is not significantly affected by a change in a disk diameter from D = 60 to 120 nm (see inset in Figure 2c).[29] To illustrate the spectral broadening effect in more detail, we show the relationship between the resonance energy and the full width at half-maximum (Γ) for a large number of different nanoholes in Figure 2c. In this plot, we utilize the spread in individual hole diameters, and thus in resonance position, in the three samples to access a more continuous range of resonance parameters. The plot clearly indicates a more or less linear relationship (i.e., $[\Gamma] \approx 1.96 - 0.77E_{res}$ [eV]) even within each sample. For 60 and 107 nm nanoholes, the average dephasing times, which are related to the resonance widths through $[\Gamma] = 2\hbar/\tau$, are 2.4 and 1.7 fs, respectively, which can be compared to $\tau \approx 2.2$ fs for disks of D = 60−120 nm. The difference is most notable for the larger diameters, where both the hole and the disk resonances are well bellow the interband region of gold (i.e., $\tau_{disk} \approx 1.3\tau_{hole}$ for $D \approx 110$ nm).

4.2. Electric Field Distribution around Single Nanoholes. In order to further our understanding of the nature of the resonant hole excitations, the near-field distribution around single holes excited at resonance are necessary, see Figure 3. The BEM plots were made at 1.96 eV for the D = 60 nm hole (Figure 3a−c) and at 1.65 eV for the D = 107 nm hole (Figure 3d−f; i.e. at energies corresponding to the scattering maxima of Figure 2b). At a distance of 5 nm above the metal surface, the *E*-field distribution exhibits clear electric dipole patterns for both hole sizes, Figure 3, panels b and e. If the *E*-field is plotted 20 nm above the nanoholes instead, the dipolar pattern is lost more quickly for the smaller hole, compare Figure 3, panels a and d, similar to the case of plasmonic nanoparticles, for which the spatial extension of the dipolar near-field component is essentially determined by particle size.[32] The maximum *E*-field enhancement is observed close to the hole edges (i.e., $|E|/|E_0|$ = 4.1 and 5.5 for the 60 and 107 nm holes, respectively) because it is at these positions that the charge accumulation associated with the dipolar excitation is the largest. The calculations are thus fully consistent with the idea that the hole resonance can be viewed as a localized electric dipole plasmon (i.e., a "hole LSP"). However, the *E*-field enhancement around the nanoholes is small in comparison with nanodisks[33] and nanorings[34] of similar dimensions, but this is not surprising, considering the lower quality factor of the hole resonance compared to disk or ring LSPs.

The near-field plots can also be used to estimate the decay length of the *E*-field inside the holes, which is an important parameter in, for example, biosensing applications.[21,22] If the field decay is assumed to be exponential {i.e., $E(r) \propto E_0(\exp(x/\delta) + \exp(-x/\delta))$}, we obtain decay length of the order of ~30 and ~40 nm in the *x* direction toward the center of the hole for the 60 and 107 nm holes, respectively. This is in reasonable agreement with experimental data for 60 nm holes, which yielded a surface-averaged value of $\delta \approx 10-20$ nm.[22]

4.3. Generation of SPPs by Single Nanoholes. To study possible LSP-SPP coupling effects in more detail, we used scattering-type near-field scanning optical microscopy. This experiment confirmed that the nanoholes indeed act as point sources of SPPs, see Figure 4, panels a and b. The measurement is qualitatively similar to NSOM experiments on isolated holes in optically thick gold films.[18] As can be seen from the figure, the emanating SPPs are more pronounced in the direction of electric field polarization, and the cone-like SPP fringes have different periods across the *x* axis (defined as the projection of the incident wavevector along the surface), see Figure 4c.

Close to the hole, the near-fields at the metal probe tip are likely to disturb the LSP. For this reason, we do not consider

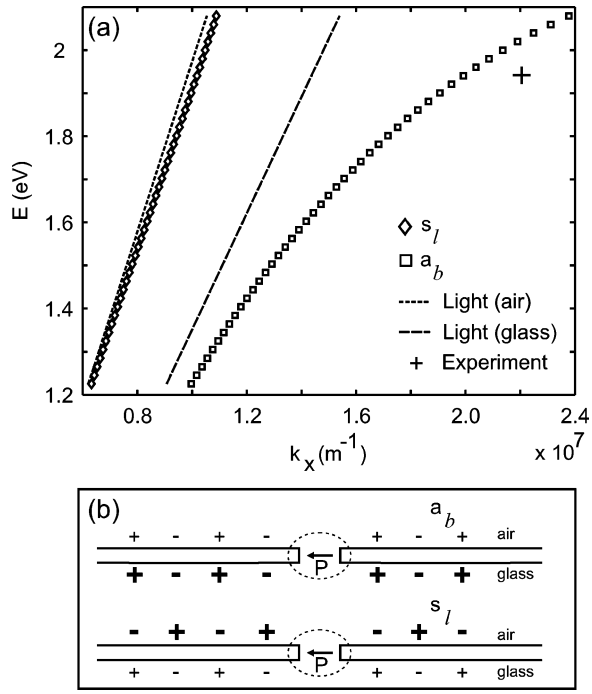

Figure 5. (a) Dispersion relations for the antisymmetric bound (a_b) and the symmetric leaky (s_l) modes in a 20 nm thick gold film on a glass substrate in air obtained using the reflection pole method. The dashed lines show the light lines at grazing incidence in the two media. The "+" symbol is the experimental value of k_{SPP} obtained from the Figure 4a. (b) Illustration of a dipole moment created by a nanohole, *P*, and the charge distributions created by the a_b and the s_l modes.

the immediate vicinity of the hole in the following and adjust the gray-scale for optimal visibility of the fringes further away from the hole. Similar to surface phonon polariton probing,[35] the fringes far from the hole can be explained by interference of the incoming field E_i with the surface plasmon polariton wave E_{SPP}, see Figure 4d. The signal amplitude we detect, E_t, is proportional to the coherent sum of the incident field and the surface plasmon field {i.e., $E_t = E_i + E_{SPP} \propto (1 + A \exp[i(k_{spp} - k\cos(\theta))x + \varphi_0])$}, where A is the SPP field amplitude relative to the incoming field E_i, is the SPP wavevector, and $[\varphi]_0$ is the phase of the SPP relative to the incoming field E_i at the source. The fringe spacing in the forward direction is then $2\pi/(k_{SPP} - k\cos(\theta))$, which is larger than it is in the opposite ($-x$) direction, $2\pi/(k_{SPP} + k\cos(\theta))$. The SPP wavelengths estimated from the fringe periodicity in the $+x$ and $-x$ propagation directions were found to be 304 ± 10 nm and 266 ± 10 nm, respectively. The average value, $\lambda_{SPP} \approx 285$ nm, is less than half the free space wavelength, which rules out classical diffraction effects as the source of the fringe pattern.

Figure 5a shows the calculated SPP dispersion relations for a 20 nm Au film on glass ($n_{glass} = 1.52$) in air ($n_{air} = 1.00$) within the energy range of interest. We consider here the Fano modes that are physically admissible[36] (i.e., the symmetric leaky (s_l) and the antisymmetric bound (a_b) modes). The film only supports one bound mode, as the gold film thickness is below the cutoff ($\approx$50 nm) for the symmetric bound mode.[36] As can be seen from the figure, the dispersion curve for the a_b mode is well below the light-lines in either media; that is, the SPP wavelength is much shorter than for any free-space light-waves of the same energy. This means that direct excitation of the a_b mode, for example via prism coupling, is prohibited and the SPP mode can only be launched through defect coupling.

The SPP wavelength of the a_b mode at the free space wavelength of $\lambda = 633$ nm is found to be $\sim$308 nm, which is in good agreement with the value $\lambda_{SPP} \approx 285$ nm estimated from the s-NSOM experiment (see "+" symbol in Figure 5a). We note that the a_b mode is characterized by a charge displacement pattern that consists of equal sign charges on the two interfaces,[37] which results in an antisymmetric field distribution, see Figure 5b. The charge distribution around the hole thus coincides with that of an electric dipole, which explains why the hole LSP mode can couple to the a_b-SPP mode. In addition to the a_b mode, the structure also supports the s_l mode. In this case, charges of opposite sign occurs at the two interfaces, resulting in a symmetric field distribution, see Figure 5b. The s_l mode should therefore not couple to a dipolar hole plasmon.

From the results above, the most plausible explanation of why the hole resonance has a shorter lifetime than the corresponding disk LSP is simply that it has access to an additional decay channel in the form of surface plasmon polaritons. Calculations of the energy dissipation of a dipole emitter close to a semi-infinite Au slab (not shown) indicate that the quantum efficiency for SPP generation (i.e., the probability that an emitted photon launches a SPP wave instead of propagating to the far field) is of the order several tens percent for the energy range of interest here.[38] Although the LSP-SPP coupling strength will depend sensitively on the detailed geometry of the hole−film system, similar to the case of a spherical metal particle outside a thin metal film,[39] it is clear that SPP interactions will have a large impact on the lifetime of any localized resonance with an energy that overlaps with the SPP density of states (DOS). In a solid-state physics picture, the broadening caused by LSP-SPP coupling corresponds to the imaginary part of a LSP self-energy, whereas the real part corresponds to a frequency shift. The DOS of the relevant SPP mode (the a_b-mode) peaks at high energies ($\sim$2.3 eV), and we therefore expect that the hole LSP mode is pushed toward lower energies compared to the LSP of a disk of the same size, which is not renormalized by LSP-SPP coupling. This picture can thus qualitatively explain why hole LSP's are red-shifted compared to disks.

5. Summary

In this paper, we have studied the optical properties of single nanosized holes prepared by colloidal lithography in optically thin (20 nm) gold films. The holes exhibit a resonance that red-shifts and broadens when the hole diameter is increased. These features could be well reproduced by electrodynamic simulations based on the boundary element method. The calculated *E*-field distribution around the nanoholes displayed a clear electric dipole character, which supports our previous assignment of the hole resonance to a localized surface plasmon resonance.

The shorter dephasing time of the hole LSP compared to disk plasmons was interpreted as an effect of LSP-SPP coupling. This picture was supported by near-field microscopy of an isolated 60 nm nanohole, which showed that the hole indeed acts as a scattering center for SPPs. The fringe period obtained from the s-NSOM image was found to be $\sim$285 nm for an illumination wavelength of 633 nm, which agrees with the wavelength of the antisymmetric bound SPP mode of a homogeneous 20 nm Au film on glass.

Acknowledgment. Funding for this work was provided by the Swedish Research Council and the Swedish Foundation for Strategic Research. We thank George C. Schatz, William L. Barnes, Peter Nordlander, W. Andrew Murray, Joan Alegret, and Rashid Zia for stimulating discussions and suggestions.

Note Added after ASAP Publication. This article was published ASAP on December 19, 2006. An additional affiliation has been added for one of the authors. The correct version was published on December 22, 2006.

References and Notes

(1) Ebbesen, T. W.; Lezec, H. J.; Ghaemi, H. F.; Thio, T.; Wolff, P. A. *Nature* **1998**, *391*, 667−669.
(2) Kim, T. J.; Thio, T.; Ebbesen, T. W.; Grupp, D. E.; Lezec, H. J. *Opt. Lett.* **1999**, *24*, 256.
(3) Lezec, H. J.; Degiron, A.; Devaus, E.; Linke, R. A.; Martín-Moreno, L.; García-Vidal, F. J.; Ebbesen, T. W. *Science* **2002**, *297*, 820−822.
(4) Levene, M. J.; Korlach, J.; Turner, S. W.; Foquet, M.; Craighead, H. G.; Webb, W. W. *Science* **2003**, *299*, 682−686.
(5) Devaux, E.; Ebbesen, T. W.; Weeber, J.-C.; Dereux, A. *Appl. Phys. Lett.* **2003**, *83*, 4936−4938.
(6) Brolo, A. G.; Gordon, R.; Leathem, B.; Kavanagh, K. L. *Langmuir* **2004**, *20*, 4813−4815.
(7) Brolo, A. G.; Arctander, E.; Gordon, R.; Leathem, B.; Kavanagh, K. L. *Nano Lett.* **2004**, *4*, 2015−2018.
(8) Williams, S. M.; Rodriguez, K. R.; Teeters-Kennedy, S.; Stafford, A. D.; Bishop, S. R.; Lincoln, U. K.; Coe, J. V. *J. Phys. Chem. B* **2004**, *108*, 11833−11837.
(9) Barnes, W. L.; Dereux, A.; Ebbesen, T. W. *Nature* **2003**, *424*, 824−830.
(10) Lezec, H. J.; Thio, T. *Opt. Express* **2004**, *12*, 3629−3651.
(11) García de Abajo, F. J. *Opt. Express* **2002**, *10*, 1475−1484.
(12) Degiron, A.; Lezec, H. J.; Yamamoto, N.; Ebbesen, T. W. *Opt. Commun.* **2004**, *239*, 61−66.
(13) Degiron, A.; Ebbesen, T. W. *J. Opt. A: Pure Appl. Opt.* **2005**, *7*, S90−S96.
(14) Zakharian, A. R.; Mansuripur, M.; Moloney, J. V. *Opt. Express* **2004**, *12*, 2631− 2648.
(15) Hillenbrand, R.; Keilmann, F.; Hanarp, P.; Sutherland, D. S.; Aizpurua, J. *Appl. Phys. Lett.* **2003**, *83*, 368−370.
(16) Chang, S. H.; Gray, S. K.; Schatz, G. C. *Opt. Express* **2005**, *13*, 3150−3165.
(17) Popov, E.; Neviere, M.; Boyer, P.; Bonod, N. *Opt. Commun.* **2005**, *255*, 338−348.
(18) Yin, L.; Vlasko-Vlasov, V. K.; Rydh, A.; Pearson, J.; Welp, U.; Chang, S. H.; Gray, S. K.; Schatz, G. C.; Brown, D. B.; Kimball, C. W. *Appl. Phys. Lett.* **2004**, *85*, 467−469.
(19) Wannemacher, A. *Opt. Commun.* **2001**, *195*, 107−118.
(20) Prikulis, J.; Hanarp, P.; Olofsson, L.; Sutherland, D.; Käll, M. *Nano Lett.* **2004**, *4*, 1003−1007.
(21) Dahlin, A.; Zäch, M.; Rindzevicius, T.; Käll, M.; Sutherland, D.; Höök, F. *J. Am. Chem. Soc.* **2005**, *127*, 5043−5048.
(22) Rindzevicius, T.; Alaverdyan, Y.; Dahlin, A.; Höök, F.; Sutherland, D.; Käll, M. *Nano Lett.* **2005**, *5*, 2335−2339.
(23) Hanarp, P.; Sutherland, D. S.; Gold, J.; Kasemo, B. *Colloids Surf. A: Physicochem. Eng. Aspects* **2003**, *214*, 23−36.
(24) Keilmann, F.; Hillenbrand, R. *Phil. Trans. R. Soc. London A* **2004**, *362*, 787−805.
(25) García de Abajo, F. J.; Howie, A. *Phys. Rev. Lett.* **1998**, *80*, 5180.
(26) García de Abajo, F. J.; Howie, A. *Phys. Rev. B* **2002**, *65*, 115418.
(27) Sepulveda, B.; Lechuga, L. M.; Armelles, G. *J. Lightwave Technol.* **2006**, *24*, 945−955.
(28) Anemogiannis, E.; Glytsis, E.; Gaylord, T. K. *J. Lightwave Technol.* **1999**, *17*, 929− 941.
(29) Hanarp, P.; Käll, M.; Sutherland, D. S. *J. Phys. Chem. B* **2003**, *107*, 5768−5772.
(30) Bohren, C. F.; Huffman, D. R. *Absorption and scattering of light by small particles;* John Wiley & Sons: New York, 1983.
(31) Johnson, P. B.; Christy, R. W. *Phys. Rev. B* **1972**, *6*, 4370−4379.
(32) Gunnarsson, L.; Rindzevicius, T.; Prikulis, J.; Kasemo, B.; Käll, M.; Zou, S.; Schatz, G. C. *J. Phys. Chem. B* **2005**, *109*, 1079−1087.
(33) Kelly, K. L.; Coronado, E.; Zhao, L. L.; Schatz, G. C. *J. Phys. Chem. B* **2003**, *107*, 668−677.
(34) Aizpurua, J.; Hanarp, P.; Sutherland, D. S.; Käll, M.; Bryant, G. W.; García de Abajo, F. J. *Phys. Rev. Lett.* **2003**, *90*, 057401−1.
(35) Huber, A.; Ocelic, N.; Kazantsev, D.; Hillenbrand, R. *Appl. Phys. Lett.* **2005**, *87*, 081103.
(36) Burke, J. J.; Stegeman, G. I.; Tamir, T. *Phys. Rev. B* **1986**, *33*, 5186−5201.
(37) Sernelius, B. E. *Surface Modes in Physics*; Wiley: New York, 2001.
(38) García de Abajo, F. J. et al., in preparation.
(39) Le, F.; Lwin, N. Z.; Steele, J. M.; Käll, M.; Halas, N. J.; Nordlander, P. *Nano Lett.* **2005**, *5*, 2009−2013.